Journal of Hydrology 517 (2014) 1089–1106

Contents lists available at ScienceDirect

Journal of Hydrology

journal homepage: www.elsevier.com/locate/jhydrol

Modeling coupled surface water – Groundwater processes in a small mountainous headwater catchment

Hendrik M. Voeckler [a,b,*], Diana M. Allen [b], Younes Alila [a]

[a] Department of Forest Resources Management, University of British Columbia, Vancouver, BC V6T 1Z4, Canada
[b] Department of Earth Sciences, Simon Fraser University, Burnaby, BC V5A 1S6, Canada

ARTICLE INFO

Article history:
Received 10 March 2014
Received in revised form 8 June 2014
Accepted 12 June 2014
Available online 21 June 2014
This manuscript was handled by Corrado Corradini, Editor-in-Chief, with the assistance of Aldo Fiori, Associate Editor

Keywords:
Headwater catchment modeling
Recharge to deep bedrock
Steep mountainous terrain
MIKE SHE

SUMMARY

Hydrological models for headwater catchments have typically excluded deep groundwater flow based on the assumption that it is a negligible component of the water budget. This study tests this assumption using a coupled surface water–groundwater model to explore the potential contribution of deep groundwater recharge to the bedrock in a snowmelt-dominated headwater catchment (Upper Penticton Creek 241) in the Okanagan Basin, British Columbia. Recharge to the bedrock is estimated at ~27% of the annual precipitation over the period 2005–2010, recognizing the uncertainty in this estimate due to data limitations, parameter uncertainty and calibration errors. A specified outward flux from the catchment boundary within the saturated zone, representing ~2% of the annual water budget, was also included in the model. This outward flux contributes to cross-catchment flow and, ultimately, to groundwater inflow to lower elevation catchments in the mountain block. This modeling exercise is one of the first in catchment hydrologic modeling within steep mountainous terrain in which the bedrock is not treated as impermeable, and in which recharge to the bedrock and discharge to the surrounding mountain block were estimated.

1. Introduction

Hydrological processes in mountains have been studied for many decades at a variety of scales. Most studies, however, have simulated only hydrologic processes in the thin soil layer above the bedrock surface (e.g. Merritt et al., 2006; Kuras et al., 2011, 2012; Thyer et al., 2004; Whitaker et al., 2003; Schnorbus and Alila, 2004, among many others) or deeper groundwater processes in the saturated zone (e.g. Gleeson and Manning, 2008; Welch and Allen, 2012; Welch et al., 2012). In recent years, there has been growing focus on groundwater-related processes in the catchment (e.g. Mau and Winter, 1997; Constantz, 1998; Freer et al., 2002; Wenninger et al., 2004; Tromp-van Meerveld et al., 2008; Tague and Grant, 2009; Lowry et al., 2010; Kosugi et al., 2011; Haught and Meerveld, 2011; Penna et al., 2011), which has led to growing interest about coupled surface water and groundwater processes in mountains (Wilson and Guan, 2004).

In mountain catchments, there is some degree of partitioning of groundwater recharge whereby a portion of the recharge is diverted back to the stream network and a portion contributes to deep groundwater flow in the mountain block. Subsurface discharge to streams may be as shallow groundwater or subsurface stormflow through alluvial cover materials, and/or as deep groundwater through fractured bedrock (e.g. Anderson et al., 1997; Montgomery et al., 1997; Wohl, 2000; Tsujimura et al., 2001; Freer et al., 2002; Uchida et al., 2003; Wenninger et al., 2004; Tromp-van Meerfeld et al., 2007; Hopp and McDonnell, 2009). Tromp-van Meerfeld et al. (2007) estimated that up to 21% of total streamflow in the Panola Mountain Research Watershed in Georgia, USA was derived from deep groundwater. Water recharged within the mountain catchments that does not "re-surface" as discharge to mountain streams (or stream valley sediments), forms deep groundwater flow systems within the bedrock mountain (Forster and Smith, 1988; Gleeson and Manning, 2008). This deep groundwater discharges to valley-bottom alluvial aquifers at the mountain front, producing diffuse (through the bedrock massive) or focused (through fault zones) mountain block recharge (Wilson and Guan, 2004). But estimates of mountain block recharge are highly uncertain, ranging from 0.2% to 38% of annual precipitation (Wilson and Guan, 2004; Manning and Solomon, 2005). Estimating this deep groundwater flux is one objective of this study.

Modeling approaches involving coupling surface water (SW) processes and groundwater (GW) processes may provide a means

* Corresponding author at: Department of Forest Resources Management, University of British Columbia, Vancouver, BC V6T 1Z4, Canada. Tel.: +1 778 862 1792.
E-mail address: hendrik_voeckler@yahoo.de (H.M. Voeckler).

http://dx.doi.org/10.1016/j.jhydrol.2014.06.015
0022-1694/

for understanding groundwater processes and interactions between groundwater and surface water, and quantifying recharge and the various components of the water balance in mountainous areas. In this study, a coupled surface water–groundwater model is developed for a small headwater catchment (Upper Penticton Creek 241 – UPC 241 catchment) in British Columbia, Canada with the aim of exploring the role of deep groundwater flow in the catchment dynamics. The code selected is MIKE SHE (Danish Hydraulic Institute (DHI) 2007). MIKE SHE is a physically distributed modeling system, which is able to simulate all the major physical processes of the hydrologic cycle through six process-oriented components: evapotranspiration (ET), snowmelt, overland/channel flow, unsaturated and saturated subsurface flows, and exchange between aquifers and rivers. To our knowledge, with the exception of Sahoo et al. (2006), MIKE SHE has not been used in steep mountainous headwater catchments. Therefore, one of the objectives of this study is to investigate the performance of MIKE SHE for simulating coupled hydrological processes at the catchment scale. This is accomplished by comparing time series for the various monitoring datasets and examining the partitioning of groundwater recharge to both the stream network and deep groundwater flow using the model water balance. The modeling results are also compared to the results of previous modeling efforts (Thyer et al., 2004; Kuras et al., 2011) using the surface water model DHSVM (Wigmosta et al., 1994) for the same catchment. More generally, the model performance is compared to other recently published modeling studies using MIKE SHE (e.g. Hammersmark et al., 2008; Sultana and Coulibaly, 2010; Rahim et al., 2012; Sahoo et al., 2006). All of these studies, besides Sahoo et al. (2006), simulated watersheds that were relatively flat (i.e., with little change in elevation within the catchment) and demonstrated acceptable modeling performances concerning the components simulated.

2. The study area

The study area is the Upper Penticton Creek watershed (UPC 241), which is a headwater tributary catchment to the regional Penticton Creek first order watershed (Fig. 1). It is located in the Okanagan Highland alpine zone approximately 26 km northeast of the City of Penticton, British Columbia (BC), Canada. The UPC 241 catchment has a drainage area of about 4.7 km^2 and ranges in elevation from ~1600 to 2025 m above sea level (masl). It is located immediately below the local mountain crest, which has an elevation of about 2100 masl. It is plateau dominated, with 75% of the area having slopes less than 30%. The lower 1.5 km^2 of the watershed is relatively flat (<7% slope). The remaining upper area is substantially steeper and accounts for 45% of the catchment's relief (Kuras, 2006; Thyer et al., 2004). Fig. 2 shows the topography of the headwater catchment, the stream network, the two climate stations, the snow measurement sites, stream gauge station, as well as bedrock monitoring wells and shallow soil piezometer transects. Details concerning the available data are presented in Section 3.

The watershed is part of the Upper Penticton Creek (UPC) Watershed Experiment (Winkler et al., 2005), which was designed as a paired watershed study. Watershed scale measurements of hydrological and meteorological parameters have been conducted for pre- and post-treatment sampling periods in two logged (UPC 241, Dennis Creek) and one unlogged (UPC 240) control watershed. UPC 241, the focus of the current study, was logged in stages for comparison with the pristine adjacent watersheds. By spring 2003, ~28% of the watershed area had been clearcut logged (Thyer et al., 2004). The next, and final, treatment was in winter 2006/2007, resulting in ~47% being logged (Fig. 2).

The catchment is located within dry Engelmann Spruce Subalpine Fir (ESSF) biogeoclimatic sub-zone. Vegetation in the unlogged portion (53%) of the watershed includes mature logdepole pine (*Pinus contorta* Dougl.) with small areas of Englemann spruce (*Picea engelmanni* Parry) and sub-alpine fir (Abies *lasiocarpa*). The trees at the study site are over 100 years old and reach maximum heights of 20–26 m. The canopy densities range from 35% to 50%. The understory is composed of lichens, mosses, and shrubs (<0.5 m in height) (Kuras et al., 2011).

Thyer et al. (2004) undertook hydrologic modeling at the site using the distributed hydrological model (DHSVM – Distributed Hydrology Soil Vegetation Model) (Wigmosta et al., 1994) in order to simulate streamflow for the logged (UPC 241) and unlogged (UPC 240) catchments. Kuras et al. (2011, 2012) studied the effects of forest roads and harvesting on the hydrology of the snow-dominated headwater catchment UPC 241 also using DHSVM. Their work combined a process-based study with physically-based, distributed hydrological modeling to improve the current understanding of snow-dominated hydrology, with an examination of the impacts of forest management on such systems. The studies specifically addressed the knowledge gap in forest hydrology regarding forest roads and harvesting in snowmelt-dominated regimes.

3. Methodology

3.1. Model domain

Within MIKE SHE, the model domain is discretized horizontally into an orthogonal network of grid squares (finite difference cells) to represent the spatial variability of catchment characteristics and input data. A number of computational layers with variable thicknesses are used to describe vertical variations in the subsurface materials and their respective hydrogeological characteristics within each grid square (as discussed in detail below). Lateral flow between the grid squares is either as overland flow or subsurface flow within the saturated zone.

A 1:20 0000 digital elevation model (DEM; GeoBC, 2007) defined the topography of the UPC 241 watershed. The DEM resolution (and model cell discretization) was 30 m with a total of 5270 cells (Fig. 2). The model domain was delineated by the UPC 241 watershed boundary derived from the DEM. The vertical depth of the model was 200 m based on the depth to which the bedrock is assumed to be relatively permeable as discussed below. Fig. 3 shows a conceptual three dimensional model of the headwater catchment, including the main components: boundary conditions, discretization, unsaturated zone, saturated zone, etc. Each component, along with an overview of how the relevant processes are simulated, is described in detail in the following sections.

3.2. Meteorological data

Hourly climate data (air temperature, precipitation (rain and snow), relative humidity, short wave solar radiation, and wind speed data) were available (BC Ministry of Forests and Range BCMoFR (EP956)) for two climate stations in the UPC 214 watershed: P1 situated a low elevation in a large forest clearing (1620 m; Fig. 2) (August 1997-present), and PB situated at upper elevation in a clearcut (1900 m; Fig. 2) (September 1999-present). Details concerning instrumentation of the climate stations are given in Voeckler (2012). In addition, snow data were available from four stations (two in forested locations and two in clearcuts; at both high and mid elevation; Fig. 2). Snow data were collected three times per month during late winter and spring snowmelt of 2004 and 2005 (Winkler et al., 2005).

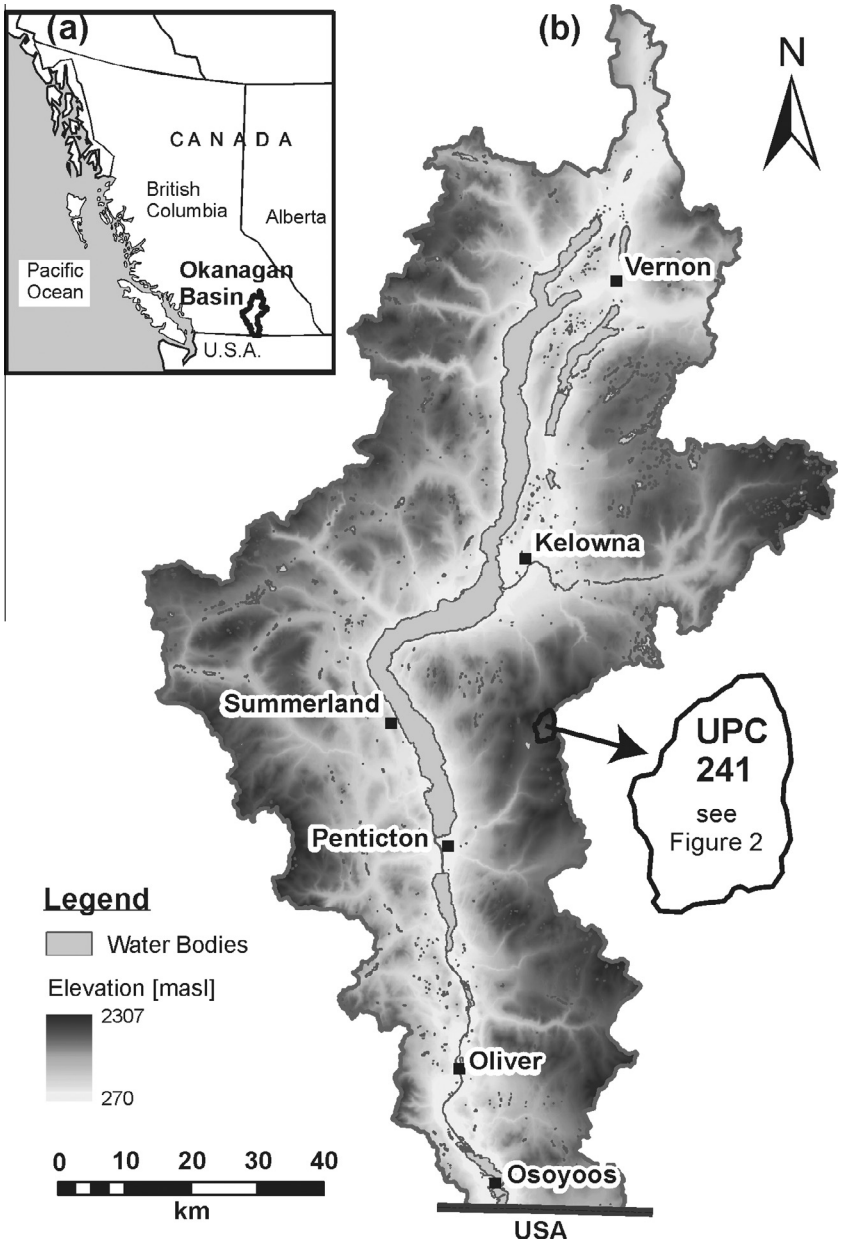

Fig. 1. Location map of the UPC 241 headwater catchment in Okanagan Basin. The inset map shows Okanagan Basin, British Columbia, Canada.

To apply the meteorological data to the model, the model domain was divided into two parts (Fig. 4a), the upper part using climate data derived from station PB and the lower part using climate data from station P1. The border between the climate zones was placed at roughly mid elevation within the watershed. In the upper zone, the topography is much steeper than in the lower zone. No precipitation gradient was applied to the site based on the similarity of precipitation records at the two climate stations. In the overlapping measurement time period (September 1999–September 2010), P1 recorded 8982 mm of precipitation, and PB 8734 mm, representing less than a 3% difference. However, due to the temperature gradient with elevation, temperatures measured at the higher elevation site (PB) are, in general, slightly lower on average by ~2 °C. Thus, air temperature within each elevation/climate zone was corrected for elevation using a temperature lapse rate of −0.24 °C/100 m according to Thyer et al. (2004). Fig. 5 shows the hourly temperature variation over four years (2007–2010) for site P1.

Fig. 5 shows the precipitation data for the period 2007–2010 for site P1. The mean annual precipitation is 750 mm, approximately half of which falls as snow. The heaviest precipitation events occur from April to the end of June. During the summer months of July and August, precipitation events decrease in number and amounts are lower. In the fall (September to November), rain events are more frequent, but not as frequent as in spring. During the winter months (November to April) most of the precipitation falls as snow (due to temperatures below 0 °C). A continuous snow cover usually lasts from late October to early June. April 1st snow water equivalent (SWE) averages about 265 mm and the late winter snowpack is normally 1–1.5 m (Kuras et al., 2011). Therefore, the model was set to include snowmelt.

The degree day method (DHI, 2007) was used to simulate snowmelt with a melting temperature set to 0 °C. The initial degree-day coefficient was set to 5.0 mm/°C/day. Model runs that included melting due to solar radiation, using typical parameter settings (e.g. radiation melting coefficient (0 mm/kJ/m^2), minimum storage

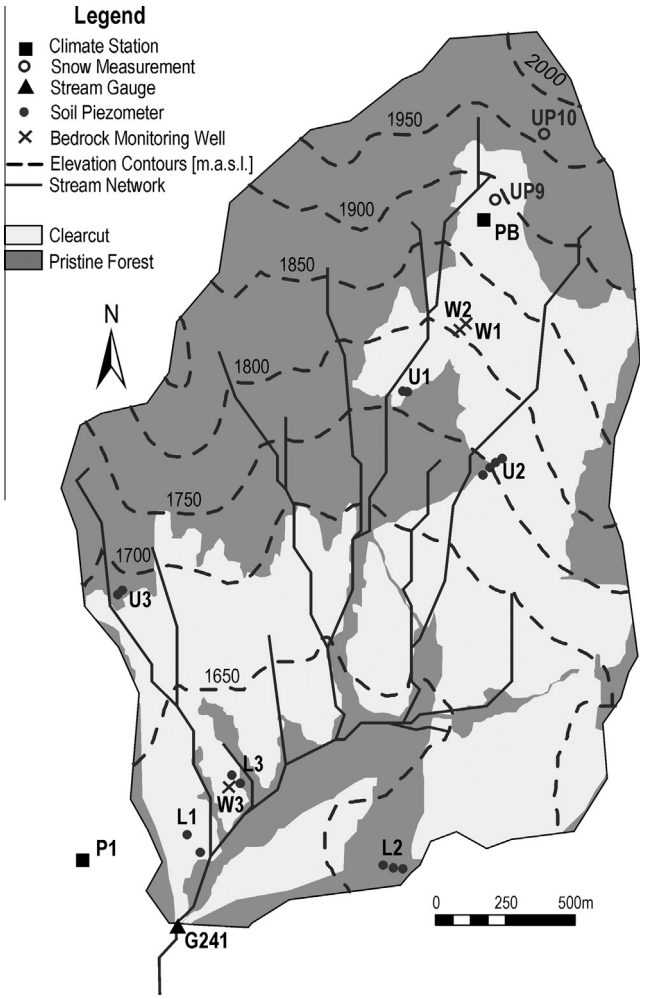

Fig. 2. Upper Penticton Creek watershed showing elevation, the stream network, and the various monitoring sites (climate stations, stream gauging stations, bedrock monitoring wells, soil piezometers and snow measurement sites).

depth (5 mm), initial snow storage in September (0 mm) maximum wet snow fraction (0) and initial total wet snow fraction (0)) gave unrealistic streamflow and SWE results. This is likely because solar radiation applies uniformly over the area represented by each climate station (both situated in open areas), and thus does not consider the effects of forested versus unforested areas. The highest daily values of solar radiation (~4000 kJ/m^2/h) are measured during the summer months and lowest daily values (<~500 kJ/m^2/h) are measured during the winter months. As shown in the results, excluding solar radiation did not appear to significantly compromise the calibration results.

Potential evapotranspiration (PET) is also needed as an input data time series file. PET was calculated using AWSET (Cranfield University, 2002) at daily time steps from the three meteorological data time series (precipitation, temperature and solar radiation) plus two additional time series data (hourly wind speed and humidity). AWSET uses the Penman–Monteith method for calculating PET (Allen et al., 1998). The maximum PET is ~6 mm/day during the summer months and the minimum PET is ~0.5 mm/day during the winter months (data not shown).

3.3. Land surface data and overland (OL) flow

Land surface data in MIKE SHE requires definition of vegetation classes. Vegetation class, representing the latest stage of logging in 2007 (47% of the watershed) was mapped in ArcGIS and imported to MIKE SHE. Seven classes were defined (Table 1 and Fig. 4b after Kuras et al., 2011). Although MIKE SHE does allow for changes in vegetation characteristics during the simulation period, to simplify the simulation, vegetation changes were not included. The implications of this are discussed further in the model calibration section. Each vegetation class was assigned a representative leaf area index (LAI) and rooting depth. Table 1 gives a description of the overstory, dominant height, LAI and rooting depth for each vegetation class (after Kuras et al., 2011). LAI and rooting depth values were not subject to calibration. Where bedrock is exposed, the LAI was assigned a zero value. LAI values for forested areas ranged from 2.5 to 4.0. A very low value of 0.5 was assigned to regenerated clearcut areas. A rooting depth (RD) value of 300 mm was assigned to all the tree classes, whereas bedrock areas and regenerated clearcut areas were assigned a smaller rooting depth of 50 mm. These parameters remained constant throughout the simulation period.

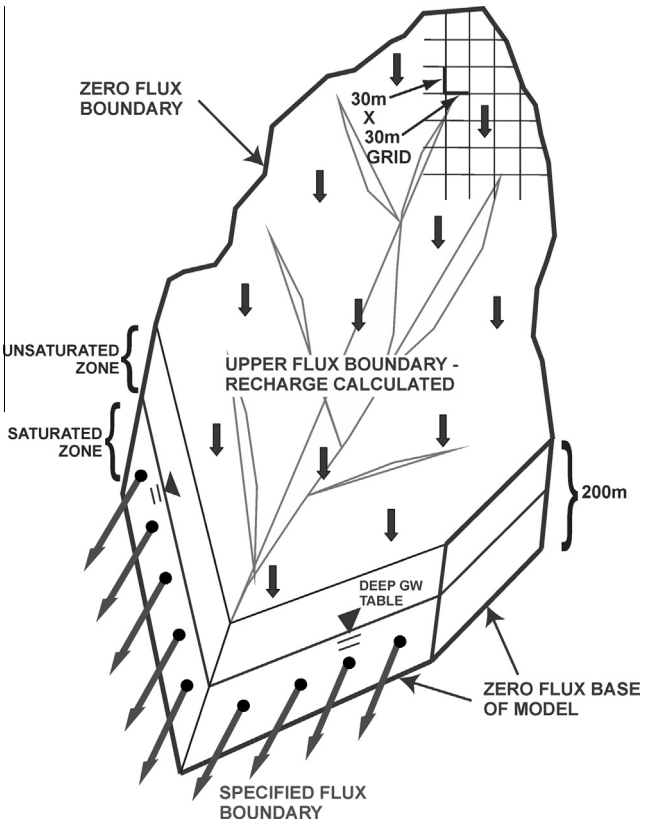

Fig. 3. Conceptual model of the UPC241 catchment, showing boundary conditions, horizontal discretization, vertical domain depth, and the unsaturated and saturated zones.

The Kristensen and Jensen equations are used to calculate actual transpiration and soil evaporation based on several evapotranspiration parameters. These include canopy interception C_{int} (mm), the gravity flow and Richards' ET parameters C1, C2, C3 (mm/day), and the root mass distribution parameter Aroot (1/m). Canopy interception is modeled as an interception storage, which must be filled before throughfall/stemflow to the ground surface takes place. C_{int} defines the interception storage capacity of the vegetation per unit of LAI (set to 0.05 mm). Values from Sahoo et al. (2006) were assigned for the three empirical coefficients, C1 (0.3 mm/day), C2 (0.2 mm/day), and C3 (20 mm/day). In the Kristensen and Jensen model, water extraction by the roots for transpiration varies over the growing season; Aroot (0.25 1/m) controls how much water will be extracted with depth.

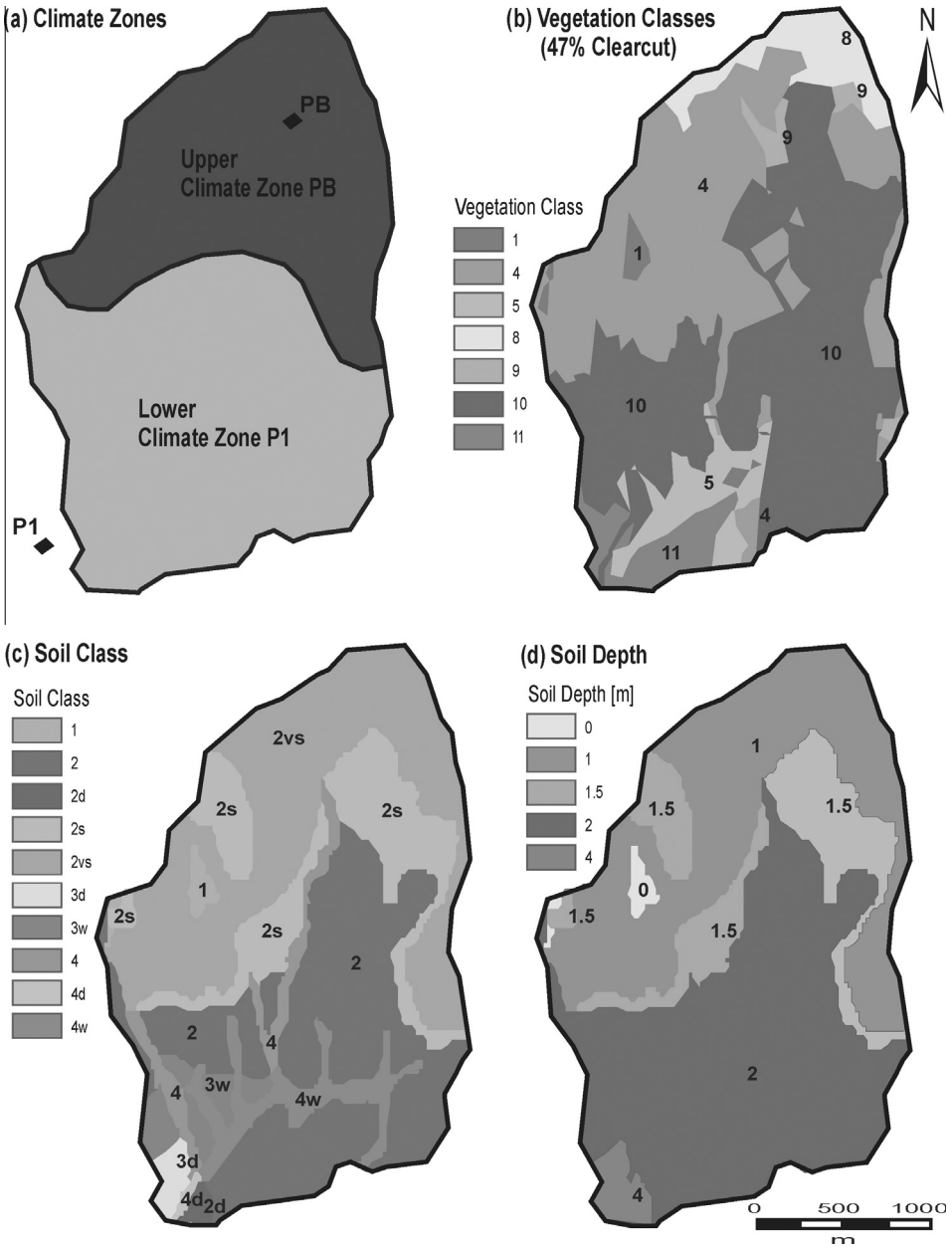

Fig. 4. Spatial datasets for the UPC 241 watershed. (a) Upper and lower climate zones. The upper zone uses the climate data measured at station PB and the lower uses climate data measured at station P1. (b) Vegetation classes at 47% logging stage. Parameters for each vegetation class are shown in Table 1. (c) Soil class. (d) Soil depth.

The St. Venant equation is solved numerically in two dimensions for overland (OL) flow. OL flow settings require Manning's n, detention storage and initial water depth. A higher value of Manning's *n* for overland flow decreases the total amount of water flowing as surface runoff and results in higher streamflow peaks. An initial value of 0.07 $m^{1/3}/s$ was assigned. Detention storage (mm) is used to limit the amount of water that can flow over the ground surface. The depth of ponded water must exceed the detention storage before water will flow as sheet flow to the adjacent cell. If detention storage is low, more water can flow over the surface resulting in higher streamflow peaks. An initial value of 2 mm was assigned. Initial water depth was 0 mm.

3.4. Unsaturated zone (UZ)

In this study, vertical flow in the soil zone is modeled using Richards' equation, which solves for pressure head variation in the unsaturated zone. Flow was calculated at each grid point. No macropore flow was included. The unsaturated zone (UZ) and saturated zone (SZ) are explicitly coupled (run in parallel).

The unsaturated zone (UZ) in MIKE SHE is the zone through which the water table rises and falls (Fig. 6). In the higher and steeper areas of the catchment, the actual water table lies within the bedrock at some depth below the soil zone. Surface water infiltrates either directly into the fractures in the bedrock or runs off as overland flow across the steep hillslopes. In the lower, flatter riparian areas of the catchment, the water table is generally shallow and lies within the soil zone. Here, groundwater discharges from the bedrock into the soils and streams. The initial model setup assigned only the soil layers to the unsaturated zone while the bedrock was assigned strictly to the saturated zone; however, during the simulation the water table fell below the depth of the unsaturated zone in the higher and steeper areas of the catchment and the model did not converge. To overcome this problem,

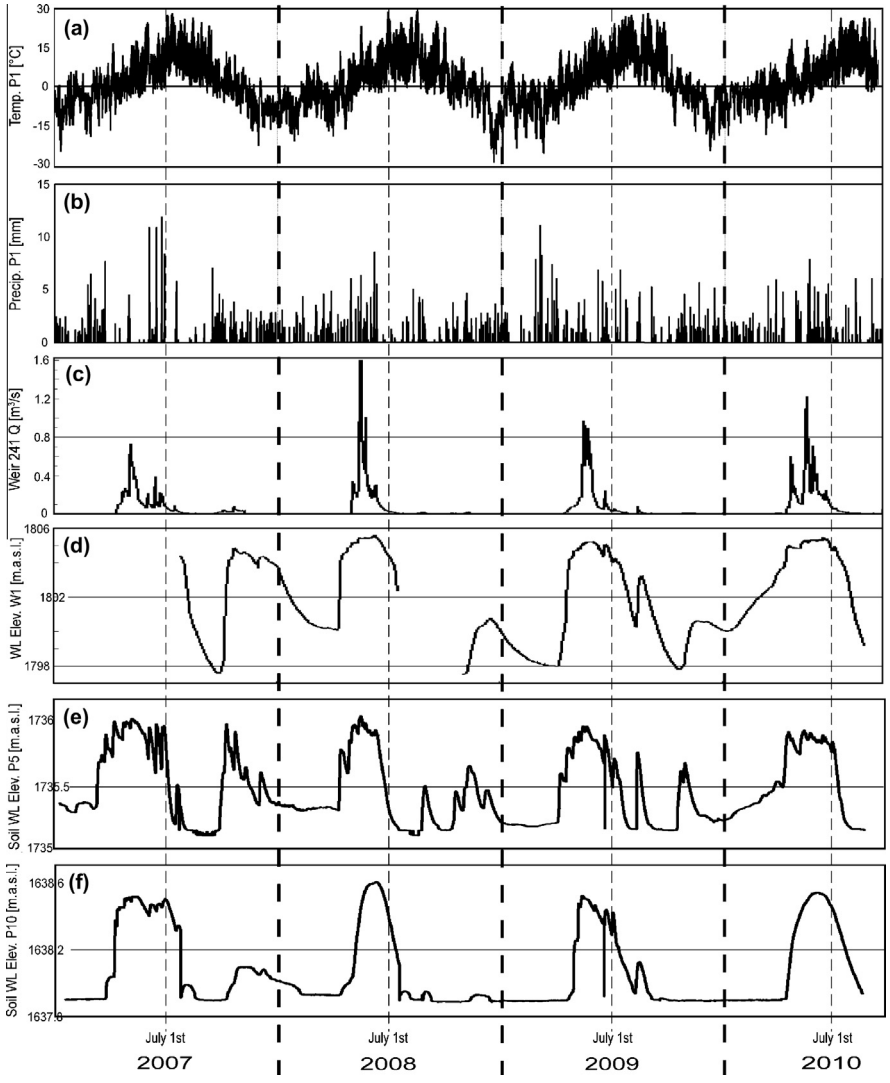

Fig. 5. Time series of hourly temperature and precipitation at site P1, discharge at the 241 weir, water level elevation in observation well W1, and water level in piezometers P5 and P10. The locations of all sites are shown in Fig. 2.

Table 1
Physical characteristics of vegetation classes (MIKE SHE input data) (data after Kuras et al., 2011).

Class	Overstory description	Dominant height (m)	LAI (m^2/m^2)	Rooting depth (mm)
1	Bedrock	N/A	N/A	50
4	Lodgepole pine	20	4.0	300
5	Lodgepole pine	25	4.0	300
8	Englemann spruce	23	2.4	300
9	Englemann spruce	26	3.8	300
10	Clearcut	N/A	N/A	50
11	Regenerated clearcut	0.6	0.5	50

bedrock was also assigned to the unsaturated zone to a depth of 200 m, and to a depth of 200 m in the saturated zone domain (Fig. 6).

Accordingly, the unsaturated zone had three layers: layers 1 and 2 of the soil (L1 and L2, respectively), and the bedrock. The thickness of L1 was set to 0.3 m, and the thickness of L2 was variable (ranging from 1 to 4 m) as indicated in Table 2. The deepest soils (up to 4 m depth) are in the riparian zones low elevation, close to the stream outlet. At higher elevations, and where slopes are steep, the soils become thinner. In total, ten UZ soil profiles were defined based on soil class. If bedrock was exposed at surface, then only one "soil" layer was defined (from 0 to 200 m). One or two soil layers could also be present above the bedrock, depending on location in the watershed. The upper soil layers were discretized vertically into 0.2 m cells, and the bedrock into 0.5 m cells.

Soil classes and soil depths were determined from field mapping by Hope (2001) as shown in Fig. 4c and d, respectively. Soils are derived from glacial tills and coarse-grained, granitic rock (Hope, 2001). Surface soil layers are mostly coarse sandy loam, although areas with fine sandy loam or silty loam occur as well. Subsurface soil layers are mostly loamy sand and are slightly compacted at depths below 0.6 m. The clay content of the soil is low, whereas the coarse fragment content is high. The initial saturated hydraulic conductivity (K_{sat}) values (m/s) and porosity of each soil class were from Thyer et al. (2004), which had been based on textural analyses and model calibration. The initial K_{sat} and porosity values for bedrock were assumed uniform with depth and were based on Voeckler and Allen (2012) (as discussed below). K_{sat} was adjusted during model calibration. Parameter values for the van Genuchten model for unsaturated flow (saturated water content, residual water content, wilting point pressure, field capacity, empirical constant alpha (cm^{-1}) and empirical constant, n) were

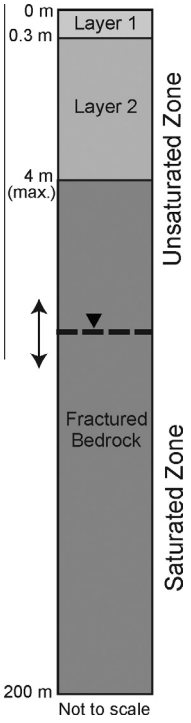

Fig. 6. Representation of the unsaturated zone (UZ) and the saturated zone (SZ).

based on soil type according to van Genuchten (1996) and published empirical relationships (Rawls et al., 1993), and were kept constant during calibration (Table 2). The van Genuchten parameter values for the fractured bedrock were based those used by Smerdon et al. (2009).

Shallow groundwater levels have been measured with piezometers positioned along transects (see Fig. 2 for piezometer transect locations) since the freshet of 2005. Piezometer transects were situated strategically throughout the watershed in order to give an overall representation of shallow groundwater fluctuations. Transects were positioned to follow the downslope routing of flows along hillslopes (approximated by surface topography). For transect design, it was important that no topographic disconnections (rises or depressions) exist between the piezometers. The change in elevation between each piezometer along a transect was large to prevent overlap, ranging from about 3 to 6 m. Piezometers were drilled using a hand auger to a depth beyond the pre-melt season perched water table. To reduce the influence of local stream stage on shallow groundwater levels, the bottoms of piezometers located in riparian zones were set approximately 15 cm above the water surface (at full bank stage) of proximal streams. All piezometers are completed in the lower, compacted soil layer L2. The installation of the piezometer transects was done during summer low flow season to assure that the depths of the piezometers was sufficient to capture perched water level fluctuations throughout the monitoring period. Odyssey capacitance water level probes (Dataflow Systems Pty Limited, 2014) were installed in each piezometer, and water levels were monitored continuously every 30 min. Table 3 shows the details of all piezometer transects located in upper (U) and lower elevation (L) of the watershed.

At higher elevations in the watershed (e.g., transect U2), the water levels are shallow and reflect perched saturated flow above the water table (i.e. the perched water table is disconnected from the saturated zone). The remaining piezometers, which are located in the lower elevation and flatter riparian zones close to the streams, are most likely connected to the saturated zone. Here, deep bedrock groundwater discharges to the streams and the depth to the saturated zone is relatively shallow. Fig. 5 shows the water level fluctuations measured in two piezometers (P5 along transect U1, P10 along transect L2) over the 2007–2010 period.

3.5. Saturated zone (SZ)

The Boussinesq equation (Boussinesq, 1872) is used to represent subsurface flow in the saturated zone and is solved implicitly (iteratively) using a 3D-finite difference technique. The saturated zone (SZ) comprises crystalline bedrock consisting of mostly fractured granite and gneiss. Bedrock can be exposed at surface, but typically it underlies the soil layers as discussed in the UZ section. The bedrock layer was assigned a lower elevation of 200 m below ground surface and was discretized as a single computational layer. Initial hydraulic conductivity (K) values of $K_x = K_y = 8.1 \times 10^{-8}$ and $K_z = 7.3 \times 10^{-8}$ m/s, specific storage of ($Ss = 3.2 \times 10^{-3}$) and specific yield ($Sy = 0.01$) were assigned. Both parameters were subject to calibration. These values were derived from Voeckler and Allen (2012) using discrete fracture modeling in the study area. These values compare well to the compilation of K values for crystalline rock from modeling studies (range of $\sim 10^{-8}$ to 10^{-7} m/s; Gleeson et al., 2011). K values were assigned uniformly over the full 200 m thickness. Previous studies have suggested that K values up to approximately 150–200 m are relatively constant (Gleeson et al., 2011; Welch and Allen, 2014).

The base of the model was assigned as a no flow (zero flux) boundary. However, to allow for some component of the deep groundwater flow to exit the catchment (i.e., not be directed to the streamflow), water was permitted to leave the saturated zone of model domain along the southern lateral edges (Fig. 3). These southern edge model boundaries were assigned specified flux (non-zero) values to effectively simulate cross-catchment flow. Of course, this flux is not known, but if the groundwater system is to be calibrated along with the surface water system, then presumably there will be some constraint on the value of this flux. The initial flux estimate was −0.005 m/s over the bedrock computational layer (negative to indicate outflow). This flux was considered to be invariant with time, but in reality the flux would likely be greater during the snowmelt period. Finally, the northern, eastern and western boundaries were assigned no flow boundaries. The upper boundary of the saturated zone is a flux boundary as well, as represented by the recharge from the unsaturated zone. This flux varies in time and is computed at the interface of the unsaturated and saturated zones.

Groundwater levels were monitored in three deep monitoring wells (W1, W2 and W3) starting in July 2007 (Fig. 2). All wells are completed in the bedrock and cased through the surficial sediments. W1 and W2 are within 3 m of each other at high elevation in the catchment (W1 is 50 m deep and W2 is 30 m deep), and W3 (30 m deep) is situated at low elevation. Fig. 5 shows the groundwater level variation in W1 (the response for W2 is nearly identical). The response of W1 to precipitation lags minimally behind the responses of streamflow and shallow groundwater levels (Fig. 5). In addition, the large changes in water levels measured throughout the year in W1 and W2 indicate a strong connection between the bedrock and the overlying soil. W3 is a flowing artesian well and the water level rises above the top of the casing during the freshet period. Flowing conditions in W3 indicate that the hydraulic head is higher at depth, representing a discharge area.

3.6. MIKE 11 stream network and streamflow data

MIKE SHE uses MIKE 11 to route channel flow. The one-dimensional St. Venant equation is solved based on the complete

Table 2
Initial soil parameters for each soil or bedrock class and layer. Soil classes and depths are mapped in Fig. 4.

Soil class	Soil layer	Depth (m)	Texture[a]	Saturated hydraulic conductivity[b] K_{sat} (m/s)	Porosity[b]	Saturated water content[c]	Residual water content[c]	Constant alpha[c] (cm^{-1})	Constant[c] n	Bulk density[d] (kg/m^3)
1	1	200	N/A (bedrock)	2.9×10^{-7}	0.10	0.1	0.05	0.0036	2.75	1200
2	1	0.3	SL	8.2×10^{-4}	0.32	0.41	0.065	0.075	1.89	1000
	2	2	LS/SL	1.5×10^{-3}	0.24	0.41	0.057	0.124	2.28	1450
2vs	1	0.3	cSL	1.1×10^{-3}	0.30	0.41	0.065	0.075	1.89	1100
	2	1	LS/SL	1.5×10^{-3}	0.23	0.41	0.057	0.124	2.28	1490
2s	1	0.3	SL	9.7×10^{-4}	0.32	0.41	0.065	0.075	1.89	1000
	2	1.5	LS/SL	1.9×10^{-3}	0.23	0.41	0.057	0.124	2.28	1500
2d	1	0.3	SL	8.2×10^{-4}	0.32	0.41	0.065	0.075	1.89	1000
	2	4	LS/SL	1.2×10^{-3}	0.24	0.41	0.057	0.124	2.28	1470
3w	1	0.3	SL	7.0×10^{-4}	0.33	0.41	0.065	0.075	1.89	970
	2	2	LS	1.5×10^{-3}	0.24	0.41	0.057	0.124	2.28	1450
3d	1	0.3	SL	8.8×10^{-4}	0.32	0.41	0.065	0.075	1.89	1000
	2	4	LS	1.5×10^{-3}	0.24	0.41	0.057	0.124	2.28	1450
4	1	0.3	SiL	8.8×10^{-4}	0.35	0.45	0.067	0.02	1.41	850
	2	2	SL/LS	6.3×10^{-4}	0.27	0.41	0.065	0.075	1.89	1280
4d	1	0.3	SiL	8.8×10^{-4}	0.35	0.45	0.067	0.02	1.41	850
	2	4	SL/LS	6.3×10^{-4}	0.27	0.41	0.065	0.075	1.89	1280
4w	1	0.3	SiL	8.8×10^{-4}	0.29	0.45	0.067	0.02	1.41	735
	2	2	SL/LS	7.7×10^{-4}	0.27	0.41	0.065	0.075	1.89	1280

[a] S: sand(y), Si: silt(y), L: loam, c: coarse.
[b] From: Thyer et al. (2004) based on model calibration or calculated using empirical relationships from Rawls et al. (1993).
[c] Values from van Genuchten (1996).
[d] Values from Kuras (2006).

Table 3
Soil piezometer details for each transect.

Transect	Well	Elevation (m)	Cover type	Hillslope position	Depth (cm)
U1	P6	1740	Clearcut edge	Hillslope	55
	P5	1736	Clearcut edge	Riparian	119.5
U2	P1	1740	Clearcut	Hillslope	70.5
	P3	1728	Clearcut	Hillslope	91.5
	P2	1721	Clearcut	Hillslope/riparian	69.5
	P4	1716	Clearcut	Riparian	105
U3	P15	1697	Forest	Hillslope	69
	P14	1678	Forest	Hillslope/riparian	89
L1	P7	1595	Clearcut	Lower depression	77
	P8	1590	Young regen	Riparian	80
L2	P9	1644	Forest	Hillslope	76.5
	P10	1638	Forest	Hillslope	70
	P11	1635	Forest	Hillslope	94
L3	P13	1628	Clearcut	Hillslope/riparian	97
	P12	1619	Clearcut edge	Riperian	95

dynamic wave formulation for simulating channel hydraulics (Thompson et al., 2004). The hydrodynamic (HD) module in MIKE 11 comprises four components: the river network, river cross sections, boundary data and HD parameters (DHI, 2005).

MIKE 11 is dynamically coupled to MIKE SHE. The exchange of saturated zone flow and overland flow is calculated implicitly using the Darcy equation, continuously updating of the overland water depth. Dynamic coupling of MIKE SHE and MIKE 11 is done through river links, which are line segments between adjacent MIKE SHE grid squares. In MIKE 11 water levels are calculated at H-points within the coupled reaches. During simulation these H-points are transferred to adjacent MIKE SHE river links. Then MIKE SHE calculates the overland flow to each river link from adjacent grid squares, as well as the river-aquifer exchange, which are later used as lateral inflows or outflows to the corresponding MIKE 11 H-points for the next computational time step (DHI, 2007).

The stream network for the watershed was originally derived by a DEM analysis with the ArcGIS Hydrology tool, which was modified using a GPS field survey to capture details of the stream network (Kuras, 2006, Fig. 2). Boundary conditions were assigned to the end of each stream: closed boundaries were set to all the upstream ends of each branch, whereas a water level boundary was assigned to the downstream end at the main outlet of the watershed where the stream gauge is located. This water level boundary was assigned a time series of water level (stage). River cross sections were assigned along each stream using data from the stream survey (Kuras, 2006). The HD parameters included a global value of Mannings' n, which typically range from 0.01 (smooth channels) to 0.10 (thickly vegetated channels). An initial value of 0.03 $m^{1/3}/s$ (Soultana and Coulibaly, 2010) was assigned. The leakage coefficient for stream–aquifer exchange (m/s) defines a loss of water from the river to the groundwater (DHI, 2007). An initial value of 1×10^{-5} m/s (Thompson et al., 2004) was assigned and later adjusted during calibration.

At the outlet of the watershed, the Water Survey of Canada (WSC) installed and maintains a hydrometric station (08NM241 – renamed to G241 in this study). Hydrometric data have been measured since 1983, with data taken roughly bi-monthly throughout the flow seasons of the simulation years. Stream stage is recorded hourly in real time. Stream discharge (m^3/s) was calculated using an existing rating curve. Daily stream discharge data for the period 2007–2010 are shown in Fig. 5. Snowmelt dominates the annual hydrograph and the freshet peak typically occurs in late spring with 170–630 mm of water flowing from the watershed annually. The WSC considers streamflow measurements accurate to 10% (steam flow error estimate).

3.7. Model calibration and validation

For calibration, including the spin-up period, the simulation was set to run for about 14 years, starting on August 1st 1994 until September 9th 2010. The measured climate time series started in August 1997; therefore, three repeated years of climate data (from 1997 to 2000) were added to the beginning of the measured time series to allow for the model to start in 1994. During this spin-up period of about 10 years (1994–2004) the saturated zone water level (as shown by well W1 in Fig. 7) drops down continuously, since the initial water table elevation of the saturated zone was set to 0 m. From the year 2004 onward, the aquifer response appears to reach a stable state (the deep groundwater levels are no longer consistently declining) (Fig. 7). It is noted, however, that the precipitation was quite variable through the period 2003–2006, which may partially explain the variable deep groundwater levels.

The water years 2004–2008 (i.e. October 1st 2003 to September 30th 2008) were used for model calibration. Model calibration first focused on snow water equivalent (SWE) using observations for a forest and clearcut location (UP12, UP11) at mid elevation, and for each of a forested and clearcut location (UP9, UP10) in an upper elevation area of the catchment. Because snow data were only available for 2004–2005 (i.e. October 1st 2003 to September 30th 2005), this period was used for calibrating snowmelt. The degree-day coefficient was adjusted during calibration to observed SWE and streamflow. Table 4 shows the initial snowmelt calibration parameters and the final calibrated values. The resulting combination of snowmelt parameters was used for all further calibration runs.

The second phase of calibration, which was non-trivial, involved calibrating the model to observed stream discharge measured at the stream gauge (G241), pressure heads in the piezometers, and bedrock groundwater levels in the wells for the water years 2005–2008 (i.e. October 1st 2004 to September 30th 2008). This required simultaneous adjustment of overland flow parameters (Manning number and detention storage) and channel flow parameters (Manning number for streamflow and leakage coefficient for stream–aquifer exchange) in tandem with the hydraulic conductivities of the unsaturated and saturated zones, the specific storage of the bedrock aquifer, and the groundwater flux exiting the domain. MIKE SHE does not have a parameter estimation module; therefore, manual calibration was required. To do this, the overall shape of the response at each monitoring site, as well as the model fit, was recorded. The final parameters for the calibrated model are shown in Table 4.

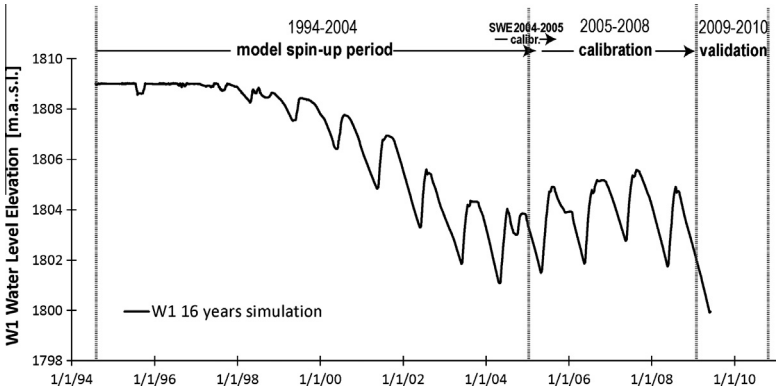

Fig. 7. Deep bedrock aquifer response of W1 for a 16 year simulation, showing the identified model spin-up period and the years used for calibration and validation.

Table 4
Initial and final calibration parameter values of the coupled MIKE-SHE MIKE 11 flow model. Only those parameters that were adjusted during calibration are shown. Ranges are reported for soil K_{sat} as soils in each layer vary spatially across the watershed.

Model	Parameter	Initial calibration value	Final calibration value
MIKE-SHE	*Snowmelt parameters*		
	Degree day coefficient (mm/°C/day)	5.0	3.3
	Overland flow parameters		
	Manning's n ($m^{1/3}/s$)	0.07	0.02
	Detention storage (mm)	2	1
	Unsaturated zone		
	K_{sat} Soil Layer 1 (m/s)	5.8×10^{-4}–1.1×10^{-3}	8.2×10^{-8}–1.1×10^{-7}
	K_{sat} Soil Layer 2 (m/s)	5.8×10^{-4}–1.1×10^{-3}	6.3×10^{-5}–1.9×10^{-4}
	K_{sat} Bedrock (m/s)	2.9×10^{-7}	2.2×10^{-7}
	Saturated zone		
	$K_x = K_y$ (horizontal) (m/s)	8.1×10^{-8}	3.2×10^{-7}
	K_z (vertical) (m/s)	7.3×10^{-8}	2.2×10^{-7}
	Specific storage Ss (m^{-1})	3.2×10^{-3}	1.0×10^{-5}
	Specific Yield Sy ()	0.01	0.01
	Outflux from saturated zone (m/s)	-5×10^{-3}	-2×10^{-3}
MIKE 11	Manning's n for channel flow ($m^{1/3}/s$)	0.03	0.05
	Leakage coeff. (river-aquifer) (m/s)	1.0×10^{-5}	1.0×10^{-5}

The validation period for the model included the years 2009–2010 (October 1, 2009 to September 9). For both model calibration and validation, the model fit was assessed using the R correlation coefficient and the Nash–Sutcliffe Efficiency (NSE) by comparing time series data for SWE, streamflow, pressure head and deep groundwater level at model cells corresponding to observation points.

4. Results

With the exception of snowmelt results, which are shown for 2004–2005, the model simulation results for streamflow, and selected deep groundwater levels and pressure heads in the soil zone are shown for a period January 1, 2007 to September 20, 2010, spanning the calibration (2005–2008) and validation (2009–2010) periods. The statistics are also reported in the respective sections below for this period. Where possible, the results are compared with those of Kuras et al. (2010), who used the DHSVM model to simulate the same watershed.

4.1. Snowmelt

In general, the snowmelt was reasonably well simulated. Fig. 8 shows the snow measurements (as SWE) at the sites, together with the simulated graphs for the snowmelt calibration period for U9 and UP10. The model fit is better for the clearcut sites at site UP9 at upper elevation ($R = 0.95$; NSE = 25) (Fig. 8a) and at the clearcut site UP11 at mid elevation ($R = 0.91$; NSE = 0.71) (results not shown), compared to the forested locations at UP10 at high elevation ($R = 0.89$; NSE = 0.62) (Fig. 8b) and at UP12 at mid elevation ($R = 0.90$; NSE = 0.49) (results not shown).

Compared to the DHSVM model results of Kuras et al. (2011), the SWE results using MIKE SHE for the forested location were not as good, but results for clearcuts were similar. DHSVM uses a two-layer energy-balance model including a forest radiation balance to simulate SWE (Wigmosta et al., 1994), in which clearcut and forest snow albedo are included. The snow albedo is a measurable reflection coefficient and is different for snow accumulation in forested and clearcut areas. In contrast, MIKE SHE uses a modified degree-day method, which does not account for different melting conditions within different vegetation covers. Thus, one limitation of the MIKE SHE model in this study is how snowmelt is simulated.

4.2. Streamflow

Fig. 9a shows the simulated and measured discharge at G241 for the period 2007–2010. Overall, the results are very good. Peak flows are slightly underestimated in 2007/08, but even the very high flows in 2008/09 are reproduced. These results are reflected in the model fit parameters ($R = 0.69$; NSE = 0.42) over the period January 1, 2001 to September 20, 2010. These model fit values are lower than those achieved by Kuras et al. (2011) using DHSVM (average NSE = 0.90 over the four year simulation period 2002–2005).

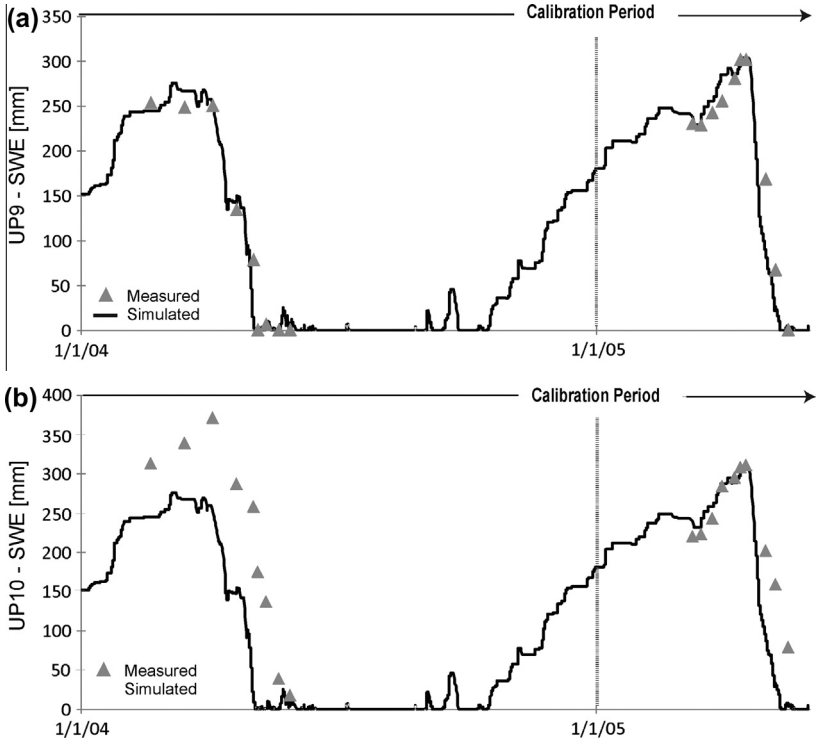

Fig. 8. Measured and simulated SWE graphs at (a) site P9 in an upper elevation clearcut area of the watershed and (b) site UP10 in an upper elevation forested area of the watershed for the period 2004–2005. The vertical gray line defines the beginning of the calibration period for all other hydrologic variables.

4.3. Deep groundwater levels

Overall, the deep groundwater levels simulated by the model are realistic for a mountainous watershed. Fig. 10 shows the simulated heads for the saturated zone during the high spring snowmelt season of 2009. Heads are highest in the upper portions of the watershed and decline toward the watershed outlet. The total range in groundwater level elevation is ~1640 to 2040 masl. Over the full range in elevation in the model, the average difference between the simulated and measured heads is less than 0.1%.

Simulated bedrock groundwater levels in W1 (and W2) are of similar magnitude to observed groundwater levels, but the timing of peaks is inconsistent (Fig. 9b). The results for W2 are not shown, but because the wells are within 3 m of each other, they lie within the same model grid cell so the simulation results are identical. The simulated water levels show only a single annual peak, which occurs during late summer. The observed heads show two peaks; one in late May (corresponding to snowmelt) and the other in early November (corresponding to fall rains). The simulated heads are interpreted to be delayed relative to the expected snowmelt response, and the fall rain events are not captured by the model. Model fit is generally poor for W1 (R = −.008, NSE = −1.72) and W2 (R = −0.86, NSE = −10.77).

While there is a strong similarity between the responses in W1 and W2, the response at W3 is different. Well W3 is located close to the outlet of the watershed at low elevation. Due to its low elevation and short surface casing height, this well flows during the spring snowmelt period (i.e., the observed water levels are uniform from late April to August – see Fig. 9c). The simulated response at W3 shows a single seasonal peak around mid-June, which is generally mid-way through the uniform heads period (Fig. 9c). Thus, the timing is very well represented at this well, but the mean hydraulic head is about 3 m lower than observed (R = −.069, NSE = −4091). No comparisons to the DHSVM model can be made, since it did not include the bedrock.

4.4. Pressure heads in the soil zone

Fig. 9d shows the simulated and measured responses of the pressure heads in piezometer P5. A pressure head of zero corresponds to the depth of the data logger at the bottom of the piezometer. The shape of the response curve is smoother compared to observed, and the response is slightly delayed (by a few days on average) relative to observed (Fig. 9d). The overall results for all 15 soil piezometers suggest that the model is generating pressure heads that are slightly too low in most areas of the catchment. The simulated pressure heads in piezometers along transects U2 (P1, P2, P3, P4) and L2 (P9, P10, P11) are underestimated relative to observed by ~0.5 to 1 m. These transects are located in hillslope areas, away from streams (see Fig. 2). The pressure heads are also too low by ~0.25 to 1 m) along transects U1 (P5, P6), U3 (P14, P15) and at one piezometer along L1 (P7) (represented here by P5 in Fig. 9d). These transects are generally either in riparian areas or in low areas (Fig. 2). Along L3 (P12, P13) and at P8 (L3), the simulated heads are too high by ~0.25 to 1 m, and water seeps at surface (horizontal flat lines in the simulated pressure head graphs). Overall, the piezometers have very statistically poor results (R ranges from −1 to 0.59 with an average of −0.12; NSE values for all piezometers are negative). However, the dynamics of shallow water table are reasonably well simulated.

Kuras et al. (2011) simulated shallow groundwater dynamics in 9 of the 15 piezometers using DHSVM. Overall, results from that study reproduced shallow water levels that are visually better than the MIKE SHE model (no model fit data were reported); however, that model did not include the deep bedrock.

4.5. Water balance

The MIKE SHE water balance tool allows for extraction of detailed water balance data for the model as a whole, and in detail for the UZ and SZ for example. Here, we present the overall water

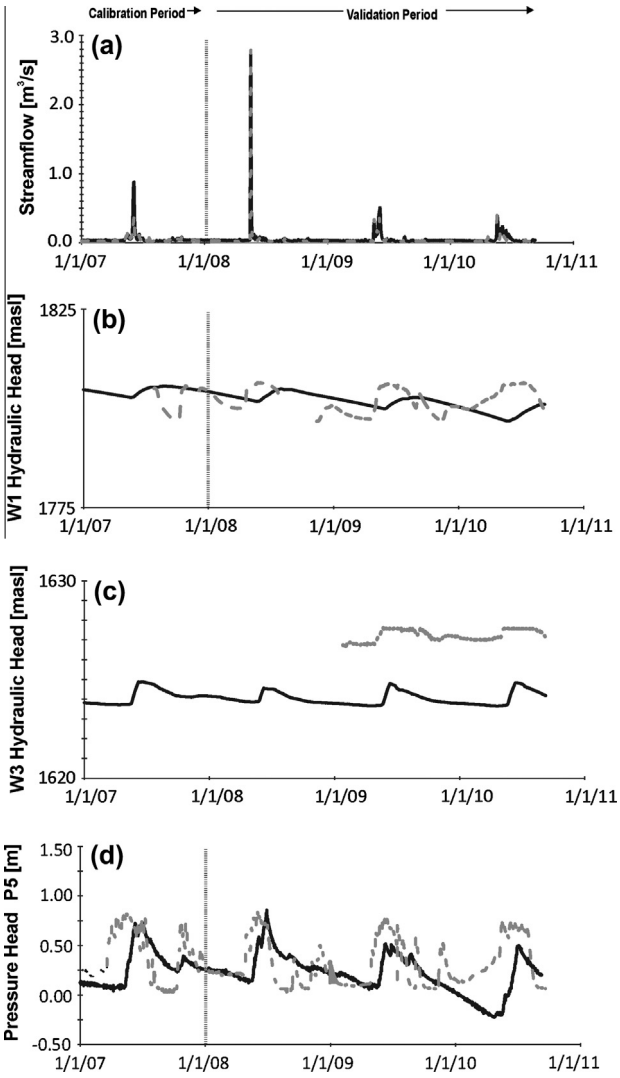

Fig. 9. Comparison of measured (gray dashed) and simulated (solid black) results for (a) streamflow at the gauge G241, (b) groundwater levels in the deep bedrock well W1, (c) groundwater levels in the deep bedrock well W3, and (d) pressure head in piezometer P5 for the period (2007–2010). The vertical gray line defines the end of the calibration period and the beginning of the validation period.

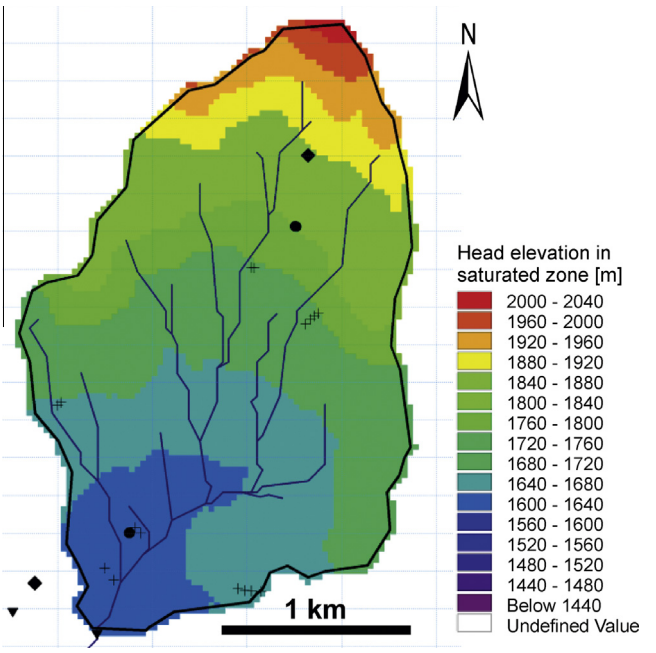

Fig. 10. Simulated hydraulic head elevations for the saturated zone during high flow spring snowmelt season of 2009 (25/05/09).

balance because the detailed water balances for the UZ and SZ incorporate numerous exchanges that are difficult to track in a simplified fashion. One of these exchanges is the recharge, which is discussed in Section 4.7.

The overall water balance is defined by:

$$\begin{aligned} &P \pm \Delta\text{Canopy Storage} - ET \pm \Delta\text{Snow Storage} \\ &\quad - \text{OL Flow to River} \pm \Delta\text{OL Storage} \\ &\quad - \text{OL Boundary Outflow} \pm \Delta\text{Subsurface Storage} \\ &\quad - \text{Baseflow to River} + \text{River to Baseflow} \\ &\quad - \text{Subsurface Boundary Outflow} \pm \text{Model Error} \end{aligned} \quad (1)$$

Table 5 shows the total water balance including the total error (mm/year) for each water year of the calibration and validation periods (2005–2010) for the major components of the water balance. Canopy storage change is not reported because it is extremely small. An additional column is added to show the recharge, which is an exchange between the UZ and the SZ, and so does not appear on the annual water balance. The water balance items, including the error, are derived from ~monthly extractions. The average of each water balance component was computed for each water year (WY) based on the monthly results. A mean annual value was then calculated from the five individual water years. In addition to the storage depth values in (mm/year) for each component of the yearly average, values in (% of precip.) are also shown in Table 5.

All the water input to the system (100%) comes from precipitation (positive values). All other components of the water balance are either fluxes out of the system, which are always negative, or storage changes, which can be positive or negative depending on individual water year. For each water year, water balance closure errors range from −12 mm/year to 46 mm/year, resulting in a 5 year average error of 16 mm/year or 2%. Within the SZ, the average water balance error was 0.0019% (not shown in Table 5), while in the UZ, the average water balance error was 1.61%.

The component of the water balance responsible for the largest volume of water lost to the system is evapotranspiration (ET), which makes up approximately 51% of the average annual water budget. Approximately 44% of the water leaves the model through the main stream at the outlet of the watershed with water entering the stream from overland (OL) flow. Small positive or negative values are reported for changes in Snow Storage and OL Storage. Baseflow to river and River to baseflow are exchanges between MIKE 11 and MIKE SHE through the H-points, where Baseflow is referenced to the MIKE SHE model, and amount to less than 1% of the water budget annually. Subsurface boundary outflow was a fixed value (specified flux), equivalent to 13 mm/y (or 2% of precipitation). This value was adjusted during a sensitivity analysis as discussed in Section 4.6.

Each of the water balance components is uncertain due to model error, calibration error, and most importantly, parameter uncertainty. For example, the estimated uncertainty for precipitation could be as high as ±50 mm (7% of total precipitation). Of the water balance components, evapotranspiration (ET) is likely the most uncertain due to the large number of parameters required to estimate potential ET and the various land surface and shallow subsurface parameters needed to simulate this process in MIKE SHE. However, similar uncertainty exists for all other components

Table 5
Total water balance for each individual water year (WY) and the yearly average (Yearly Ave.) for the calibration and validation periods spanning 2005–2010. Values in brackets represent % of precipitation for each component of the yearly average. Recharge is shown as a separate column as it is a transfer from the UZ to the SZ.

	P (mm/y)	ET (mm/y)	Snow- storage change (mm/y)	OL-flow to river (mm/y)	OL-storage change (mm/y)	OL-boundary outflow (mm/y)	Subsurface storage change (mm/y)	Baseflow to river (mm/y)	River to baseflow (mm/y)	Subsurface boundary outflow (mm/y)	Total model error (mm/y)	Recharge UZ to SZ (mm/y)
WY 05–06	703	−322	0	−321	0	−6	12	−5	0	−13	46	320
WY 06–07	653	−335	−5	−276	1	−3	−24	−5	0	−13	−12	419
WY 07–08	675	−316	0	−357	−1	−8	22	−5	0	−13	−1	122
WY08–09	699	−409	0	−269	1	−4	4	−5	0	−13	2	63
WY 09–10	664	−346	1	−269	0	−4	18	−5	0	−13	44	8
Yearly Ave. (%)	679	−346	−1	−298	0	−5	6	−5	0	−13	16	186
	100	51	0	44	0	1	1	1	0	2	2	27

P = Precipitation; ET = Evapotranspiration; OL = Overland; WY = Water Year.

Table 6
Average total water balance for 0% subsurface outflow, 2% subsurface outflow and 4% subsurface outflow. Average annual results are shown for the calibration and validation periods spanning 2005–2010. Values in brackets represent% of precipitation for each component of the average. Recharge is shown as a separate column as it is a transfer from the UZ to the SZ.

	P (mm/y)	ET (mm/y)	Snow-storage change (mm/y)	OL-flow to river (mm/y)	OL-storage change (mm/y)	OL-boundary outflow (mm/y)	Subsurface storage change (mm/y)	Baseflow to river (mm/y)	River to baseflow (mm/y)	Subsurface boundary outflow (mm/y)	Total model error (mm/y)	Recharge UZ to SZ (mm/y)
0% Subsurface outflow	679	−347 (51%)	−1 (0%)	−309 (46%)	0 (0%)	−6 (1%)	6 (1%)	−5 (1%)	0 (0%)	0 (0%)	5 (1%)	188 (35%)
2% Subsurface outflow	679	−346 (51%)	−1 (0%)	−298 (44%)	0 (0%)	−5 (1%)	6 (1%)	−5 (1%)	0 (0%)	−13 (2%)	16 (2%)	186 (27%)
4% Subsurface outflow	679	−345 (51%)	−1 (0%)	−287 (42%)	−1 (0%)	−4 (1%)	7 (1%)	−5 (1%)	0 (0%)	−26 (4%)	16 (2%)	184 (34%)

P = Precipitation; ET = Evapotranspiration; OL = Overland.

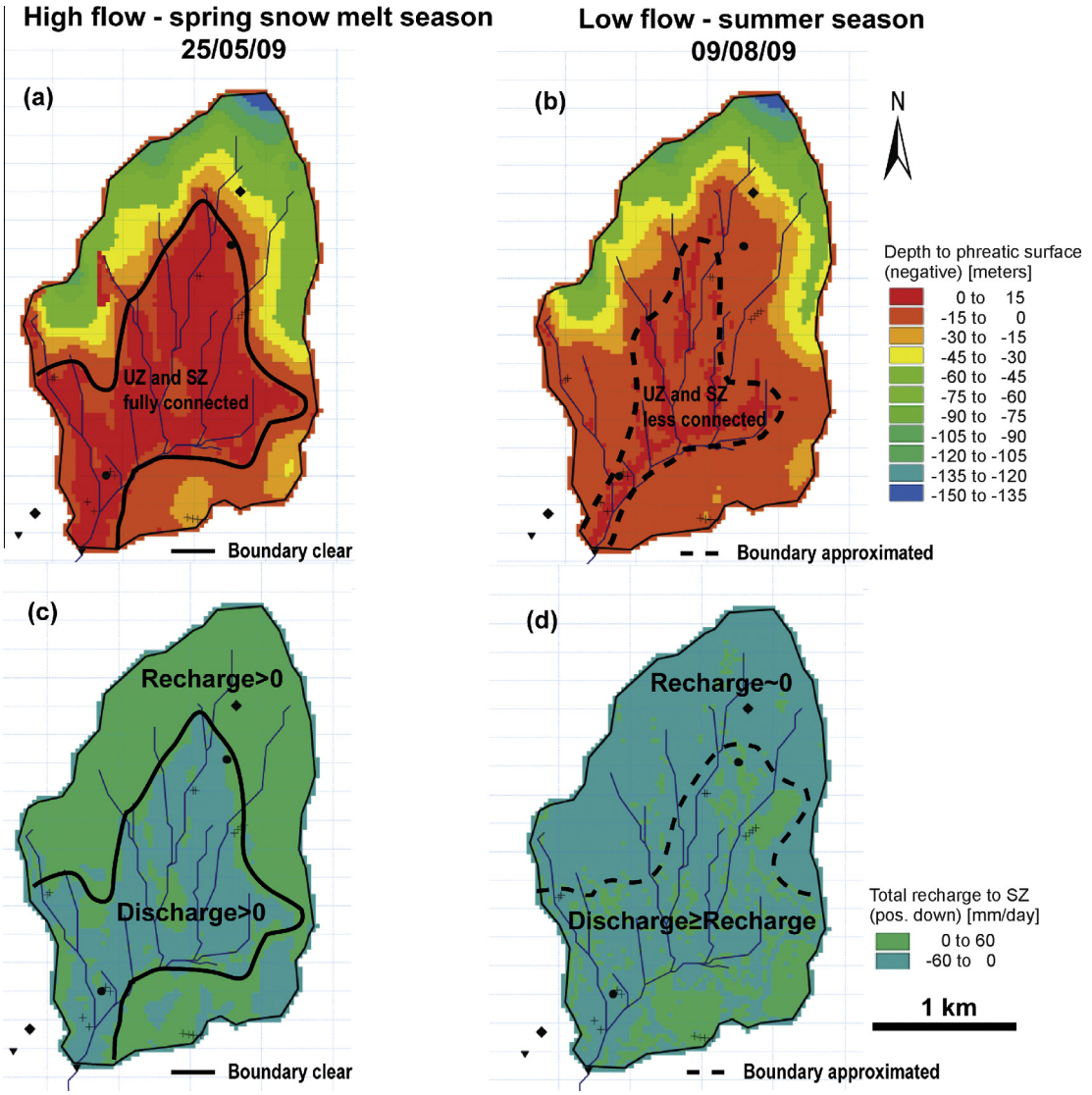

Fig. 11. Simulation results of depth to saturated zone for (a) a high flow spring snowmelt season, (b) a low flow summer season. Resulting recharge to saturated zone is shown during, (c) the high flow spring snowmelt season and (d) the low flow summer season.

of the water balance. Ideally, a complete model sensitivity analysis would be conducted to determine changes to the water balance components for different ranges of input parameters. However, such an exercise would be unwieldy for a model of this complexity. Nevertheless, a water balance sensitivity analysis was conducted for ranges in subsurface boundary outflow as discussed below.

4.6. Subsurface boundary outflow sensitivity analysis

One of the main objectives of this study was to estimate how much deep groundwater exits the system. Because the base of the model was assigned a no flow boundary, any outgoing flux was permitted to leave the model only through the lower edges of the model domain as shown in Fig. 3. Given the uncertainty in this flux value, a sensitivity analysis was performed.

Subsurface boundary outflow was varied from 0 mm/y to 26 mm/yr, representing 0% and 4% of the mean annual precipitation (Table 6). The changes in subsurface outflow were accommodated directly by changes in the streamflow (OL flow to river component of the water balance). There are minimal changes in the other components, and the overall model error for both cases is relatively unchanged (~1–2%) from the calibrated model results. In terms of model fit for streamflow, $R = 0.68$ and NSE = 0.40 for the 0% case, and $R = 0.69$ and NSE = 0.42 for the 4% case. These results suggest that, in this particular catchment, the model fit for streamflow is not particularly sensitive to the magnitude of the outward groundwater flux for the range of values tested, even though there is a loss to streamflow under the higher subsurface outflow conditions.

This subsurface boundary outflow from the headwater catchment recharges the adjacent intermediate or regional groundwater flow systems that contribute to mountain block recharge. The simulated values from this study are of the same order of magnitude as values found in the literature. For example, Welch and Allen (2012) estimated a deep groundwater flux of approximately 1.8% of annual precipitation for Daves's Creek watershed in the Okanagan. Smerdon et al. (2009) estimated a deep groundwater flux of 2.2% of annual precipitation for the BX Creek watershed. These results are remarkably similar to the values from this study. However, both of these models were strictly groundwater models with estimated groundwater recharge.

4.7. Recharge to bedrock

Based on the detailed water balances for the UZ and SZ (not shown), the UZ contributes 186 mm/year (27% of precipitation) recharge to the SZ (and the SZ receives this amount), although this

recharge amount varies considerably from year to year and ranges from 8 to 419 mm/year (Table 5 – last column). Thus, there is a significant transfer of water from the soil zone to the bedrock (recall, the SZ only consists of the bedrock).

The deep groundwater level mimics the topography (Fig. 10), but is deeper at high elevation compared to low elevation. At high elevation, the water table is positioned in the bedrock, although a perched water table can develop as reflected by the water levels in the piezometers. During the spring freshet in the snowmelt season, the soil zone becomes fully saturated in low elevation areas and there is no perched water table (Fig. 11a). Here, the bedrock water table and the "shallow" water table become one. During the summer, the water table is considerably deeper in the low elevation areas and the deep and shallow groundwater systems are less well connected (Fig. 11b). Overall, the water table dynamics in the riparian zone closely follow the runoff dynamics of the stream and the response propagates upslope (Seibert et al., 2003; Kuras et al., 2011).

During the spring snowmelt season, there is a clear boundary between the recharge area and the discharge area (Fig. 11c). The higher and steeper areas in the watershed clearly serve as recharge zones (green color) and the lower riparian areas as discharge zones (blue color). The water in the lower riparian areas seeps to the surface creating fully saturated swampy areas as indicated through the red zones in map (Fig. 11a). These swampy areas are observed at the site, but are generally restricted to areas near the watershed outlet, and do not extend as high up gradient as suggested by the simulation results.

During summer season simulated recharge is nearly zero in the upper areas of the watershed, and in the lower areas discharge nearly equals recharge, although discharge is still generally higher than recharge (Fig. 11d). This indicates that unsaturated and saturated zones interact less during the summer low flow season, while for the high flow season those zones seem to fully connect as discussed above. The boundaries between the recharge and discharge areas for the low flow season (see Fig. 11b and d) are approximated and are not as clear as the ones for the high flow season (see Fig. 11a and c).

5. Discussion

Through the calibration process and the sensitivity analysis, we learned a great deal about the model sensitivity to a range of parameters. The model was found to be very sensitive to only a few parameters, notably $K_{sat,}$ for the soils and the bedrock in the UZ. If K_{sat} for bedrock was too high, the water levels in the SZ did not decline much below the initial heads (ground surface) and it was impossible to achieve calibration of the deep groundwater levels in W1, W2 and W3. The model was less sensitive to K_z, K_y and K_z in the SZ and, in fact, there is probably room for some adjustment of the final values reported in Table 4.

Perhaps the most interesting outcome of model calibration was the need to lower the K_{sat} values of the upper soil layer by approximately two orders of magnitude relative to the initial values based on soil texture. If these values were not lowered, the generated streamflow peak was very low, despite adjustments to the detention storage and Manning's n for both overland and channel flow. (Note: the degree day coefficient snowmelt parameter also affects the peak flow, but this parameter was not varied further as it had already been adjusted during the SWE calibration with good results for the streamflow peaks.) There was no provision in the MIKE SHE code for assigning soil parameters using a time series, which would allow values to vary during the year, for example due to freezing. However, during winter in these plateau regions of the province, frost penetration to a depth of 50 cm is common (Valentine et al., 1978). Soil freezing can result in dramatic reductions in infiltration rates due to the reduction in permeability (Kane, 1980), which could explain why low K_{sat} values for the top soil layer (0.3 m depth) were needed to generate the peak flows.

While the low K_{sat} values did seem to generate reasonable streamflow peaks during spring melt, the inability to assign these values as a time series meant that the values were also low during the late spring to early fall, when in fact, the ground is not frozen during this time. As a result, there was limited permeability to rainfall. This may explain why the deep groundwater levels did not respond to the fall rains, and it might also explain why the responses in the piezometers were slightly delayed relative to observed. Of course, all of the piezometer results are likely strongly affected by the microtopography, which is no doubt inadequately represented in the model; the simulated pressure heads in the piezometers are averaged over an entire 30×30 m cell.

The low K_{sat} values assigned to soil layer 1, however, do not explain why the simulated pressure heads were generally too low across the catchment except in the lower riparian areas (transects L1 and L3) where they were too high. This points to a problem of too much deep drainage from high elevation to low. The bedrock was assigned a uniform K_{sat} value in the UZ, as well as a uniform K_z value in the SZ. K_{sat} value in the UZ was slightly higher than K_z in the SZ, which was necessary to generate the deep groundwater levels in W1 and W2 as noted above. However, if the same value was assigned to both K_{sat} and K_z, the model drained too rapidly, suggesting that the bedrock needed to have a lower K in the SZ. In reality, the bedrock does not have a uniform permeability profile. Typically, in crystalline rock there is a saprolite or highly weathered bedrock layer that extends a few metres into the unweathered fractured bedrock (Welch and Allen, 2014). This saprolite layer is more permeable than the unweathered bedrock. In essence, our model included this saprolite layer at the base of the soil zone by assigning a high K_{sat} value to the bedrock in the UZ. However, the uniform K_z of the bedrock in the SZ represented more the combined effect of the saprolite layer and a lower K bedrock unit. In the high elevations of the watershed, water percolated first through the soils, then the saprolite, and finally into the bedrock. However, in the lower parts of the watershed where the water table is near surface, the ground is close to fully saturated. Therefore, the K_z value of the bedrock in the SZ would have been activated by the model because the UZ is coupled to the SZ at the water table depth. Upon reflection, we may have achieved better results had we included a higher K zone at the top of both the UZ and SZ.

The spatially uniform K for the bedrock, whether in the UZ or SZ, is also a gross simplification of the system. The bedrock is fractured; and while at the scale of the entire catchment uniform K values may be representative (since the bedrock was treated as an equivalent porous medium), in reality, there is a network of fractures at depth which act as preferential pathways for infiltration and groundwater flow. Thus, a discrete fracture network could be used to simulate flow, but this would require a discrete fracture simulation code and the model itself would be highly parameterized. An alternative representation of the fracture rock using MIKE SHE could involve generating a heterogeneous bedrock K distribution using, for example, the FracManReservoirEdition (FRED) software (Golder Associates Ltd., 2006) and importing it into MIKE SHE as a geocellular grid. Such an approach is recommended for future study.

In this study, groundwater outflow from the SZ was assigned a specified flux because there was no other way to simulate the outflow, apart from assigning variable heads along the southern boundary. But these heads are unknown and change with time, so they are difficult to assign. Nevertheless, the sensitivity analysis did constrain the value to some degree. The results suggest that outflow via deep groundwater flow is likely a component of the water balance; however, the exact amount remains uncertain.

Varying subsurface outflow resulted in a direct change to the streamflow, even though the model fit did not noticeably change. The other components of the water balance were largely unaffected. In reality, however, the flux would likely be greater during the snowmelt period. Allowing more water out of the model during the snowmelt period relative to the summer low flow period could affect the dynamics of the deep groundwater levels (levels, timing and shape of the simulated graphs). Therefore, future work could attempt to assign a more realistic time varying flux across this boundary.

Other limitations of the study that are relate either to the code itself or our implementation of the code include:

(1) An assumption of vertical flow in the UZ, which likely does not represent hillslope flow adequately – this is a limitation of the code.
(2) Keeping the vegetation constant despite the fact that logging occurred in winter 2006/07 and keeping ET constant despite the fact that plants have an annual growth cycle – future work could examine the effects of changing vegetation and ET by specifying time series for the ET parameters.
(3) The formulation of the unsaturated flow equation (i.e., Richards' equation) has a high degree of parameter uncertainty (Scanlon et al., 2002). The van Genuchten parameters for unsaturated flow, especially those for fractured bedrock, are highly uncertain as there have been few studies of this kind to test ranges of potential values. Moreover, the process of infiltration in fractured rock remains poorly understood (e.g. Glass et al., 1995; Evans et al., 2001; Bodvarsson et al., 2003).
(4) MIKE SHE does not include culverts. Therefore, there is no provision for rapid routing of water through the road ditch-culvert system into the closest stream crossing a forest road. General consensus (e.g. Kuras, 2006; Bowling and Lettenmaier, 1997; Gucinski, 2001; Beckers and Alila, 2004) suggests that forest road segments draining directly into streams will speed up the catchment response time and contribute more to the rising limb of the hydrograph, potentially increasing peak discharge. However, this does not appear to be a problem in this study as peak streamflow was adequately simulated. The fact that culverts were included in the DHSVM model by Kuras et al. (2010) may explain why some of the model results differ between the two studies of this catchment. However, a fundamental difference is that the DHSVM model did not include deep bedrock.

6. Conclusions

Headwater catchment models in mountainous regions typically exclude deep groundwater flow in the bedrock. In these mountain settings, there can be significant interaction between the groundwater system and the surface water system. The water table is often found at depth in the fractured bedrock forming the steep hillslope areas of a catchment, while in the lower and flatter riparian zones of a catchment, the water table is very shallow and groundwater discharges to the overlying soils and streams, contributing to baseflow. The MIKE SHE modeling exercise carried out in this study is one of the first in catchment hydrologic modeling within steep mountainous terrain in which the bedrock is not treated as impermeable, and in which recharge to the deep bedrock and discharge to the surrounding mountain block are estimated.

Due to the large number of model parameters, this complex model was time intensive and challenging to calibrate. Hydraulic conductivity values of the soils and bedrock within both the unsaturated zone and the saturated zone needed to be adjusted simultaneously in order to calibrate streamflow, pressure heads in the soil zone, and the deep groundwater levels. Recognizing the uncertainty due to data limitations, parameter uncertainty and calibration error, the average water balance results over a 5 year period indicate a recharge to the bedrock of 27% of the annual precipitation. In most catchment models, the bedrock is considered impermeable.

In this study, water from the saturated zone was also permitted to leave the model domain (catchment boundary) through specified flux boundaries placed at the bottom edges of the catchment. The outward flux was invariant in time despite the likely time varying nature of the actual flux (higher perhaps during spring thaw). The estimated outward flux was approximately 2% of the annual water budget. While this is a small percentage of the overall water balance, it is consistent with other studies (Smerdon et al., 2009; Welch and Allen, 2012) and represents an important component in the context of watershed processes. Ultimately, this water contributes to deep groundwater flow entering lower elevation catchments down the mountain side, and ultimately may contribute to mountain block recharge at the valley bottom.

The overall model performance for snowmelt and streamflow was good, and was similar to other studies. However, the model performance for the unsaturated zone (pressure heads in piezometers) and the saturated zone (water table response within the deep bedrock) were not as good due to the complex nature of the interactions being simulated an uncertainty in parameters. Generally, the pressure heads were too low across the catchment, and particularly at higher elevation, and the water level responses in both the soils and the bedrock were delayed relative to observed. Also, the groundwater levels in the bedrock did not respond to fall rain events. Nevertheless, the overall dynamics were adequately represented. The model demonstrated the strong connection between the bedrock and the soils, especially in the lower riparian zones of the headwater catchment. The model also delineated reasonable recharge and discharge zones during high- and low flow seasons. Many of the shortcomings of the model can be explained by model simplifications, such as (1) time-invariant soil properties (no provision for frozen/unfrozen soils), vegetation/ET properties (no provision for annual growth cycles), and deep groundwater flux; (2) uniform hydraulic properties for the bedrock (single layer, no fractures); and (3) uncertainty in the van Genuchten parameters for the bedrock.

This study has contributed to a better understanding of groundwater processes in snowmelt dominated mountainous headwater catchments. The combined approach of including bedrock and allowing some water to leave the catchment show promise for other studies where deep groundwater flow within the mountain block constitute a greater percentage of the annual water budget, such as in arid regions.

Acknowledgements

The BC Ministry of Environment is acknowledged for providing funding to drill the observation wells; and Tim Hess at Cranfield University for providing the AWSET software for calculating reference ET. This research was supported by the Natural Sciences and Engineering Research Council of Canada (NSERC) through Discovery Grants to Diana Allen and Younes Alila, as well as a Canadian Water Network (CWN) grant. Special thanks for some additional financial assistance, great advice and field support are also owed to Dr. Rita Winkler and the entire research team at the Upper Penticton Creek Watershed Experiment.

References

Allen, R.G., Pereira, L.S., Raes, D., Smith, M., 1998. Crop Evapotranspiration. Guidelines for Computing Crop Water Requirements – FAO Irrigation and Drainage, Paper 56. FOA, Rome, 328p.

Anderson, S.P., Dietrich, W.E., Montgomery, D.R., Torres, R., Conrad, M.E., Loague, K., 1997. Subsurface flow paths in a steep, unchanneled catchment. Water Resource Res. 33 (12), 2637–2653. http://dx.doi.org/10.1029/97WR02595.

Beckers, J., Alila, Y., 2004. A model of rapid preferential hillslope runoff contributions to peak flow generation in a temperate rain forest watershed. Water Resource Res. 40 (3). http://dx.doi.org/10.1029/2003WR002582.

Bodvarsson, G.S., Wu, Y.S., Zhang, K., 2003. Development of discrete flow paths in unsaturated fractures at Yucca Mountain. J. Contam. Hydrol. 62–63, 23–42.

Boussinesq, J., 1872. Essai sur la theorie des eaux courantes. Mem. Pres. Acad. Sci., Paris 23, 680.

Bowling, L., Lettenmaier, D.P., 1997. Evaluation of the Effects of Forest Roads on Streamflow in Hard and Ware Creeks, Washington. Water Resour. Ser., Tech. Rep., Dep. Of Civ. Eng., University of Washington, vol. 155, 189p.

Constantz, J., 1998. Interaction between stream temperature, streamflow, and groundwater exchanges in alpine streams. Water Resource Res. 34 (7), 1609–1615. http://dx.doi.org/10.1029/98WR00998.

Cranfield University, 2002. AWSET Version 3.0, 2002, Cranfield University Silsoe.

Dataflow Systems Pty Limited, 2014. Odyssey Capacitance Dataloggers. <http://odysseydatarecording.com/index.php?route=product/category&path=59> (accessed February 2014).

DHI, 2005. MIKE 11: A Modeling System for Rivers and Channels-Short Introduction and Tutorial. Danish Hydraulic Institute, Denmark.

DHI, 2007. MIKE SHE User Manual: Reference Guide, vol. 2. Danish Hydraulic Institute, Denmark.

Evans, D.D., Rasmussen, T.C., Nicholson, T.J., 2001. Flow and Transport through Unsaturated Fractured Rock: An Overview, second ed. Geophysical Monograph, AGU, 196p.

Forster, C., Smith, L., 1988. Groundwater flow systems in mountainous terrain: 2. Controlling factors. Water Resources Res. 24 (7), 1011–1023. http://dx.doi.org/10.1029/WR024i007p01011.

Freer, J., McDonnell, J.J., Beven, K.J., Peters, N.E., Burns, D.A., Hooper, R.P., Aulenbach, B., Kendall, C., 2002. The role of bedrock topography on subsurface storm flow. Water Resource Res. 38 (12). http://dx.doi.org/10.1029/2001WR000872.

GeoBC, 2007. Terrain Resource Information Management (TRIM) Data. <http://archive.ilmb.gov.bc.ca/crgb/pba/trim/> (accessed January 2007).

Glass, R.J., Nicholl, M.J., Tidwell, V.C., 1995. Challenging models for fluid flow in unsaturated, fractured rock through exploration of small scale processes. Geophys. Res. Lett. 22 (11), 1457–1460. http://dx.doi.org/10.1029/95GL01490.

Gleeson, T., Manning, A.H., 2008. Regional groundwater flow in mountainous terrain: three-dimensional simulations of topographic and hydrogeologic controls. Water Resource Res. 44, 16. http://dx.doi.org/10.1029/2008WR006848, W10403.

Gleeson, T., Smith, L., Moosdorf, N., Hartmann, J., Dürr, H.H., Manning, A.H., van Beek, L.P.H., Jellinek, A.M., 2011. Mapping permeability over the surface of the Earth. Geophys. Res. Lett. 38, L02401. http://dx.doi.org/10.1029/2010GL045565.

Golder Associates Ltd., 2006. FRED (FracManReservoirEdition) Version 6.54: Redmond, Washington, Golder Associates.

Gucinski, H., 2001. Forest Roads: A Synthesis of Scientific Information, vol. 509. DIANE Publishing.

Hammersmark, C.T., Rains, M.C., Mount, J.F., 2008. Quantifying the hydrological effects of stream restoration in a montane meadow, Northern California, USA. River Res. Appl. 24, 735–753. http://dx.doi.org/10.1002/rra.1077.

Haught, D.R.W., Meerveld, H.J., 2011. Spatial variation in transient water table responses: differences between an upper and lower hillslope zone. Hydrol. Process. 25 (25), 3866–3877. http://dx.doi.org/10.1002/hyp.8354 (Special Issue SI).

Hope, G., 2001. Soil descriptions for Penticton Creek Experimental Watersheds, Report, B.C. Ministry of Forests, Kamloops Region, Kamloops, BC, Canada, 19p.

Hopp, L., McDonnell, J.J., 2009. Connectivity at the hillslope scale: identifying interactions between storm size, bedrock permeability, slope angle and soil depth. J. Hydrol. 376, 378–391.

Kane, D.L., 1980. Snowmelt infiltration into seasonally frozen soils. Cold Reg. Sci. Technol. 3, 153–161.

Kosugi, K., Fujimoto, M., Karsura, S., Kato, H., Sando, Y., Mizuvama, T., 2011. Localized bedrock aquifer distribution explains discharge from a headwater catchment. Water Resource Res. 47, W07530, doi: 1029/2010WR009884.

Kuras, P.K., 2006. Forest Road and Harvesting Effects on the Hydrology of A Snow-Dominated Catchment in South-Central British Columbia (M.Sc. thesis): Vancouver, University of British Columbia, Canada, 159p.

Kuras, P.K., Alila, Y., Weiler, M., Spittlehouse, D., Winkler, R., 2011. Internal catchment process simulation in a snow-dominated basin: performance evaluation with spatiotemporally variable runoff generation and groundwater dynamics. Hydrol. Process. 25, 3187–3203, doi: 10.1002éhyp.8037.

Kuras, P.K., Alila, Y., Weiler, M., 2012. Forest harvesting effects on the magnitude and frequency of peak flows can increase with return period. Water Resource Res. 48. http://dx.doi.org/10.1029/2011WR01705, pp. 1–1 (W01544).

Lowry, C.S., Deems, J.S., Loheide, S.P., Lundquist, J.D., 2010. Linking snowmelt-derived fluxes and groundwater flow in a high elevation meadow system, Sierra Nevada Mountains, California. Hydrol. Process. 24 (20), 2821–2833. http://dx.doi.org/10.1002/hyp.7714.

Manning, A.H., Solomon, D.K., 2005. An integrated environmental tracer approach to characterizing groundwater circulation in a mountain block. Water Resource Res. 41, W12412. http://dx.doi.org/10.1029/2005WR004178.

Mau, D.P., Winter, T.C., 1997. Estimating ground-water recharge from streamflow hydrographs for a small mountain watershed in a temperate humid climate, New Hampshire, USA. Ground Water 35 (2), 291–304. http://dx.doi.org/10.1111/j.1745-6584.1997.tb00086.x.

Merritt, W.S., Alila, Y., Barton, M., Taylor, B., Cohen, S., Neilsen, D., 2006. Hydrologic response to scenarios of climate change in sub watersheds of the Okanagan basin, British Columbia. J. Hydrol. 326 (1–4), 79–108. http://dx.doi.org/10.1016/j.jhydrol.2005.10.025.

Montgomery, D.R., Dietrich, W.E., Torres, R., Anderson, S.P., Heffner, J.T., Loague, K., 1997. Hydrologic response of a steep, unchanneled valley to natural and applied rainfall. Water Resource Res. 33 (1), 91–109.

Penna, D., Tromp-van Meerveld, H.J., Gobbi, A., Borga, M., Dalla Fontana, G., 2011. The influence of soil moisture on threshold runoff generation processes in an alpine headwater catchment. Hydrol. Earth Syst. Sci. 14 (3), 689–702. http://dx.doi.org/10.5194/hess-15-689-2011.

Rahim, E.A., Yusoff, I., Jafri, A.M., Othman, Z., Ghani, A.A., 2012. Application of MIKE SHE modelling system to set up a detailed water balance computation. Water Environ. J. 1–14. http://dx.doi.org/10.1111/j.1747-6593.2012.00309.x.

Rawls, W.J., Brakensiek, D.L., Logsdon, S.D., 1993. Predicting saturated hydraulic conductivity utilizing fractal principles. Soil Sci. Soc. Am. J. 57, 1193–1197.

Sahoo, G.B., Ray, C., De Carlo, E.H., 2006. Calibration and validation of a physically distributed hydrological model, MIKE SHE, to predict streamflow at high frequency in a flashy mountainous Hawaii stream. J. Hydrol. 327 (1–2), 94–109.

Scanlon, B.R., Healy, R.W., Cook, P.G., 2002. Choosing appropriate techniques for quantifying groundwater recharge. Hydrogeol. J. 10 (1), 18–39. http://dx.doi.org/10.1007/s10040-001-0176-2.

Schnorbus, M., Alila, Y., 2004. Forest harvesting impacts on the peak flow regime in the Columbia Mountains of southeastern British Columbia: an investigation using long term numerical modeling. Water Resource Res. 40 (W05205), 1–16. http://dx.doi.org/10.1029/2003WR002918.

Seibert, J., Bishop, K., Rodhe, A., McDonnel, J.J., 2003. Groundwater dynamics along a hillslope: a test of the steady state hypothesis. Water Resource Res. 39 (1), 1–9. http://dx.doi.org/10.1029/2002WR001404 (W1014).

Smerdon, B.D., Allen, D.M., Berg, M.A., Grasby, S.E., 2009. An approach for predicting groundwater recharge in mountainous watersheds. J. Hydrol. 365 (3–4), 156–172. http://dx.doi.org/10.1016/j.jhydrol.2008.11.023.

Sultana, Z., Coulibaly, P., 2010. Distributed modelling of future changes in hydrological process of Spencer Creek watershed. Hydrol. Process. 25 (8), 1254–1270. http://dx.doi.org/10.1002/hyp.7891.

Tague, C., Grant, G.E., 2009. Groundwater dynamics mediate low-flow response to global warming in snow-dominated alpine regions. Water Resource Res. 45, W07421. http://dx.doi.org/10.1029/2008WR007179.

Thompson, J.R., Strenson, H.R., Gavin, H., Refsgaard, A., 2004. Application of the coupled MIKE SHE/MIKE11 modelling system to a lowland wet grassland in southeast England. J. Hydrol. 293, 151–179.

Thyer, M., Beckers, J., Spittlehouse, D., Alila, Y., Winkler, R., 2004. Diagnosing a distributed hydrologic model for two high-elevation forested catchments based on detailed stand- and basin-scale data. Water Resource Res. 40, 20. http://dx.doi.org/10.1029/2003WR002414, W01103.

Tromp-van Meerfeld, H.J., Peters, N.E., McDonnell, J.J., 2007. Effect of bedrock permeability on subsurface stormflow and the water balance of a trenched hillslope at the Panola Mountain Research Watershed, Georgia, USA. Hydrol. Process. 21, 750–769. http://dx.doi.org/10.1002/hyp.6265.

Tromp-van Meerveld, H.J., James, A.L., McDonnell, J.J., Peters, N.E., 2008. A reference data set of hillslope rainfall–runoff response, Panola Mountain Research Watershed, United States. Water Resource Res. 44 (6), W06502. http://dx.doi.org/10.1029/2007WR006299.

Tsujimura, M., Onda, Y., Ito, J., 2001. Stream water chemistry in a steep headwater basin with high relief. Hydrol. Process. 15, 1847–1858. http://dx.doi.org/10.1002/hyp.243.

Uchida, T., Asano, Y., Ohte, N., Mizuyama, T., 2003. Seepage area and rate of bedrock groundwater discharge at a granitic unchanneled hillslope. Water Resource Res. 39 (1), 1018. http://dx.doi.org/10.1029/2002WR001298.

Valentine, K.W.G., Sprout, P.N., Baker, T.E., Lawkulich, L.M. (Eds.), 1978. The Soil Landscapes of British Columbia. BC Ministry of Environment, Resource Analysis Branch, 197p (accessed March 2014).

van Genuchten, M.T., 1996. Estimating unsaturated soil hydraulic properties from tension disc infiltrometer data by numerical inversion. Water Resource Res. 32 (9), 2683–2696.

Voeckler, H.M., 2012. Modeling Deep Groundwater Flow through Fractured Rock Bedrock in a Mountainous Headwater Catchment using a Coupled Surface Water–Groundwater Model, Okanagan Basin, British Columbia (Ph.D. thesis): University of British Columbia, 433p.

Voeckler, H., Allen, D.M., 2012. Estimating regional-scale fractured bedrock hydraulic conductivity using discrete fracture network (DFN) modeling. Hydrogeol. J. 20 (6), 1081–1100. http://dx.doi.org/10.1007/s10040-012-0858-y.

Welch, L.A., Allen, D.M., 2012. Consistency of groundwater flow patterns in mountainous topography: implications for valley bottom water replenishment and for defining groundwater flow boundaries. Water Resource Res. 48, W05526. http://dx.doi.org/10.1029/2011WR010901.

Welch, L.A., Allen, D.M., 2014. Hydraulic conductivity characteristics in mountains and implications for conceptualizing bedrock groundwater flow. Hydrogeol. J. http://dx.doi.org/10.1007/s10040-014-1121-5.

Welch, L.A., Allen, D.M., van Meerveld, H.J., 2012. Topographic controls on deep groundwater contributions to mountain headwater streams and sensitivity to available recharge. Can. Water Resources J. 37 (4), 349–371. http://dx.doi.org/10.4296/cwrj2011-907.

Wenninger, J., Uhlenbrock, S., Tilch, N., Leibundgut, C., 2004. Experimental evidence of fast groundwater responses in a hillslope/floodplain area in the Black Forest Mountains, Germany. Hydrol. Process. 18 (17), 3305–3322. http://dx.doi.org/10.1002/hyp.5686.

Whitaker, A., Alila, Y., Beckers, J., Toews, D., 2003. Application of the distributed hydrology soil vegetation model to Redfish Creek, British Columbia. Model evaluation using internal catchment data. Hydrol. Process. 17, 199–224. http://dx.doi.org/10.1002/hyp.1119.

Wigmosta, M.S., Vail, L.W., Lettenmaier, D.P., 1994. A distributed hydrology–vegetation model for complex terrain. Water Resource Res. 30 (6), 1665–1679.

Wilson, J.L., Guan, H., 2004. Mountain-block hydrology and mountain-front recharge. In: Hogan, J.F., Phillips, F.M., Scanlon, B.R. (Eds.), Groundwater Recharge in a Desert Environment. The Southwestern United States, Water Science and Applications Series 9. American Geophysical Union, Washington, DC, pp. 113–137.

Winkler, R.D., Spittlehouse, D.L., Golding, D.L., 2005. Measured differences in snow accumulation and melt among clearcut, juvenile, and mature forests in southern British Columbia. Hydrol. Process. 19, 51–62.

Wohl, E., 2000. Mountain Rivers. American Geophysical Union, Washington, DC, 320p.